Chapter 4

Reconfigurable Microstrip Cross Parasitic Antenna with Complete Azimuthal Beam Scanning and Tunable Beamwidth

4.1 Introduction

The antenna design proposed in Chapter 3 realized continuous beam scanning from -40° to 40° in the H-plane. This antenna design is further extended to develop multifunctional RA. The beam steering antennas are expected to have 360° scanning range with low profile and simple control mechanism. However, it is observed that in most cases, PRA designs are unable to cover the complete horizontal plane [62, 67–69, 73, 76, 78]. It is also observed that designs presented in [24, 65, 66, 74, 75, 77, 79–81] realize complete 360° coverage in the azimuth plane, but the radiated beam in the elevation plane is discretely switched. Continuous beam scanning is more beneficial over discrete beam switching in high mobility applications. To meet the requirement of such applications, main beam of the antenna needs to be precisely directed to the user terminal to increase spectral efficiency, mitigate fading effects, and reduce interference [155]. The antenna designs reported in [24, 73, 74, 79] have used PIN diodes to control mutual coupling between the driven and parasitic elements. The use of varactor diode provides several advantages such as more flexibility in controlling mutual coupling, precise scan resolution, high switching speed, and

low power consumption [115]. In addition to this, it is noted that the RA designs available in the literature either provides pattern reconfigurability or beamwidth variability in a single antenna structure. Thus, it is also worthy of investigating the applicability of parasitic antennas to design and develop multifunctional RA.

A reconfigurable cross parasitic antenna is presented in this chapter to achieve complete azimuthal beam scanning and tunable beamwidth in the E-plane and H-plane. The antenna consists of a square-shaped driven element and four size-tunable parasitic elements placed on each side of the driven element. Each tunable parasitic element is composed of a hexagonal slot loaded with two varactor diodes. Tunable parasitic element shows dual-resonance behavior and hence its effective electrical size can be controlled with respect to the driven element. Radiated beam of the cross antenna is continuously scanned in the elevation plane from θ = 0° to 10.8°, 0° to 32.4°, and 0° to 40° in ϕ = (0°, 180°), (45°, 135°, 225°, 315°), and (90°, 270°) planes respectively. Moreover, 3-dB beamwidth of the cross antenna is continuously tuned from 65° to 152° and 64° to 116° in the E-plane and H-plane respectively. The antenna shows good impedance matching in all the operating modes with -10 dB bandwidth from 2.43 to 2.47 GHz. A prototype of the antenna is fabricated to verify the simulated reflection and radiation characteristics experimentally.

The remainder of this chapter is organized as follows: Section 4.2 presents the proposed reconfigurable cross parasitic antenna design and its operating principle. This section also describes detailed mutual coupling results for different configurations of driven and parasitic elements. Simulated reflection and radiation performance of the antenna are experimentally verified, and the results are given in Section 4.3. The concluding remarks are summarized in Section 4.4.

4.2 Antenna Design

The geometrical design of the proposed antenna, along with the details of the DC biasing circuit, is described in this section. The operating principle is discussed by analyzing mutual coupling in the E-plane and H-plane of the driven element. Effect of size of the parasitic element on 3-dB beamwidth is also described in detail.

4.2.1 Antenna Configuration

The proposed reconfigurable cross parasitic antenna consists of a square-shaped driven patch and four tunable parasitic elements P1, P2, P3 and P4 arranged in the E-plane and H-plane of the driven

element, as shown in Figure 4.1(a). Geometrical parameters of the antenna are as follows (in mm): L = 28.9, L_1 = 5, L_2 = 5.5, g = 3, k = 8.95 and $L_g = W_g$ = 140. Metallic vias placed between the patch and ground plane are represented as V1 to V8. The cross parasitic antenna is designed to operate at a frequency of f = 2.45 GHz. Length of both the driven and tunable parasitic elements is L. Each tunable parasitic element consists of a hexagonal slot loaded with two varactor diodes. The positive terminal of the DC supply is connected to the metallic vias V1, V2, V3, and V4 through Coilcraft 4310LC-132KEB RF choke coil, as shown in Figure 4.1(b). The varactor diodes are grounded using high impedance transmission line of length $\lambda_g/4$ with dimensions (in mm): L_h = 16, W_h = 1.5. For this purpose, four metallic vias V5, V6, V7, and V8 are placed between the patch and ground plane. A Skyworks SMV 1233-079 varactor diode is used for the practical implementation of the proposed cross parasitic antenna. This varactor diode has variable junction capacitance from 0.84 to 5.08 pF for the corresponding reverse voltage of 15 to 0 V [153].

4.2.2 Mutual Coupling Analysis

In conventional antenna arrays, mutual coupling is undesired since it produces side lobes, grating lobes at large scan angles, and reduces the gain of the antenna. In [45], it is concluded that the mutual coupling between driven and parasitic elements can be effectively used to increase gain, increase bandwidth, and tilt the radiation pattern. Mutual coupling between driven and parasitic antenna elements depends on radiation characteristics of each element, relative separation between the elements, and orientation of each element [2]. In [156], it is shown that the mutual coupling has a significant effect on the resonant frequency, impedance bandwidth, and gain of the parasitic array. The authors also concluded that the field interaction is stronger between the non-radiating edges than the radiating edges, and parasitic elements behave like coupled multiple tuned circuits. In [157], the mutual coupling is analyzed for square, rectangular, and circular elements in E-plane and H-plane configuration. It is found that the mutual coupling in E-plane configuration is more sensitive toward a variation of distance between elements, and the coupling decreases monotonically and rapidly as the spacing increases. In [158], authors have analyzed mutual coupling in E-plane and H-plane for nearly square-shaped microstrip elements. It is concluded that the coupling between non-radiating edges is stronger as compared to radiating edges. As a result, a crossover is observed in the E-plane and H-plane coupling for nearly square-shaped microstrip elements. Mutual coupling is an important design parameter in the proposed reconfigurable cross parasitic antenna. Therefore, the mutual coupling for different configurations of driven and parasitic elements is analyzed in detail to study its effect on impedance and radiation characteristics. Ports are defined on the parasitic patches to find the mutual coupling

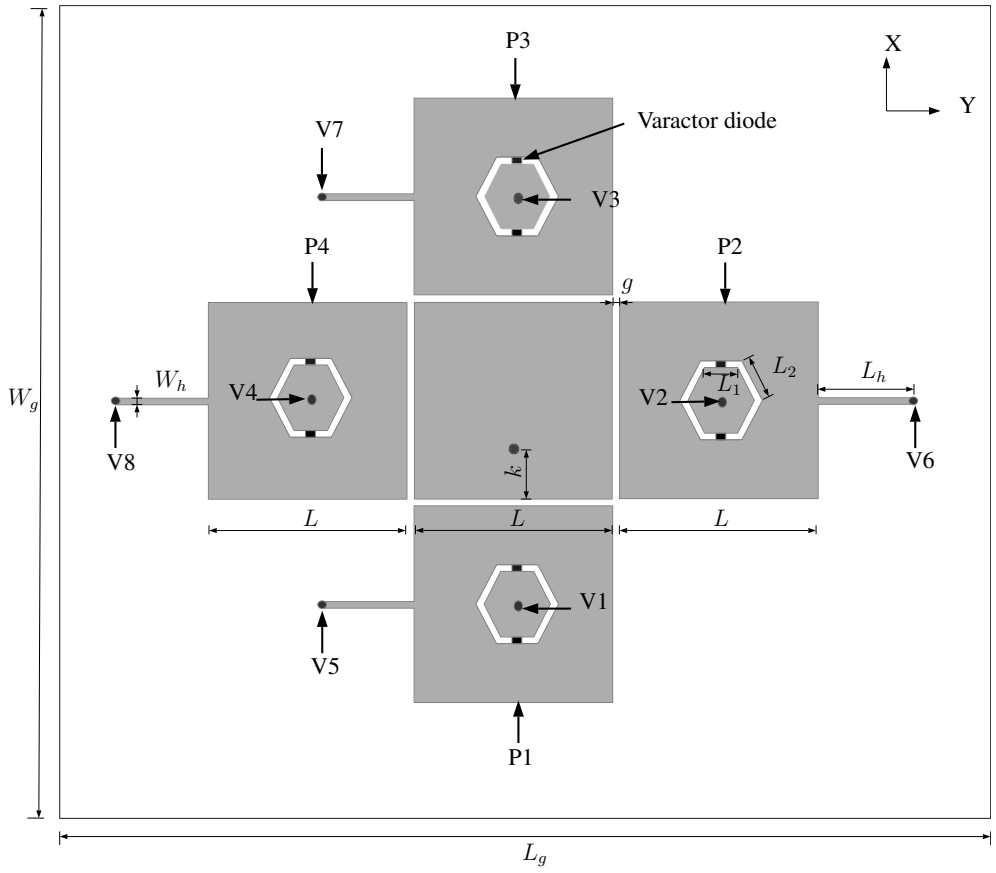

(a)

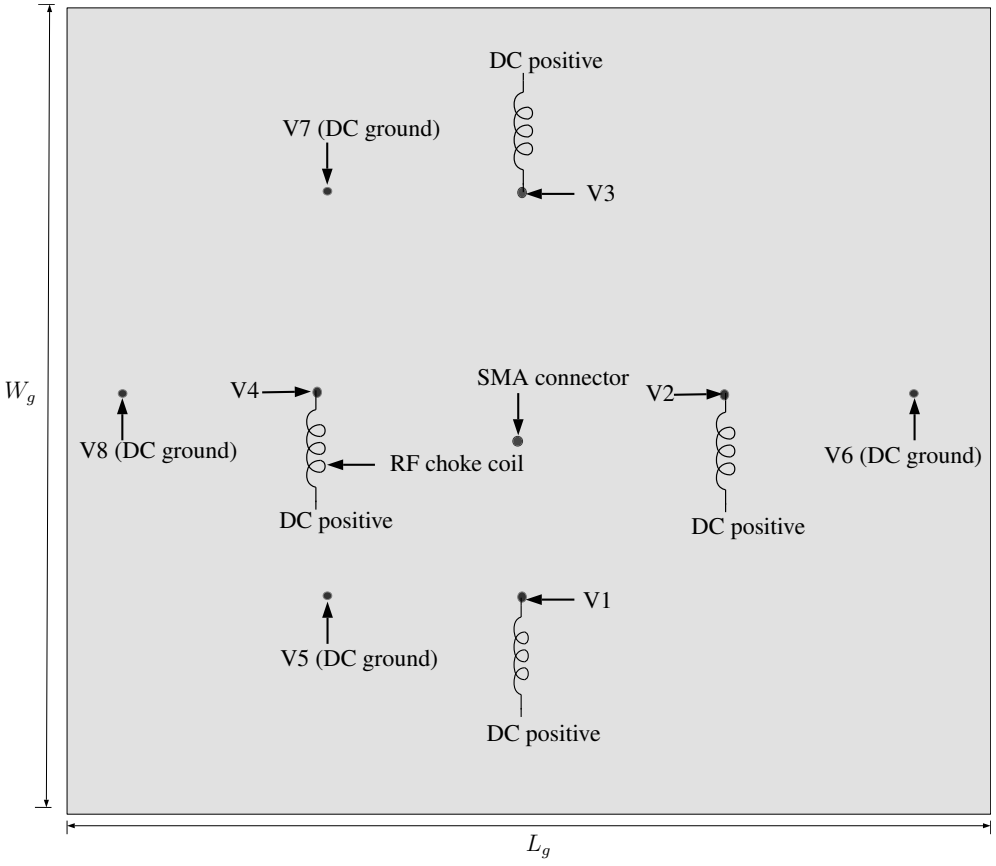

(b)

Figure 4.1. Geometrical design of the reconfigurable cross parasitic antenna (a) Front view and (b) Back view.

parameters using HFSS. The coaxial-feed driven element is excited by port 1, while port 2 defined on the parasitic element is terminated with 50 Ω impedance.

Initially, a square-shaped driven element is simulated in HFSS by separately placing one parasitic element in the H-plane and E-plane. For H-plane coupling analysis, the parasitic element is placed on the right-hand side of the driven element. For E-plane coupling analysis, the parasitic element is placed collinearly along the E-plane. Size of both the driven and parasitic elements is 28.9 mm. Distance between the driven and parasitic elements is varied from 1 mm to 12 mm to analyze the mutual coupling effects. Through simulation in HFSS, it is found that the H-plane coupling is stronger as compared to the E-plane coupling and travels over a large distance. The E-plane coupling is stronger for smaller spacings, but as the distance increases, E-plane coupling decreases very fast. Figure 4.2(a) shows the mutual coupling results for E-plane and H-plane configuration with one parasitic element.

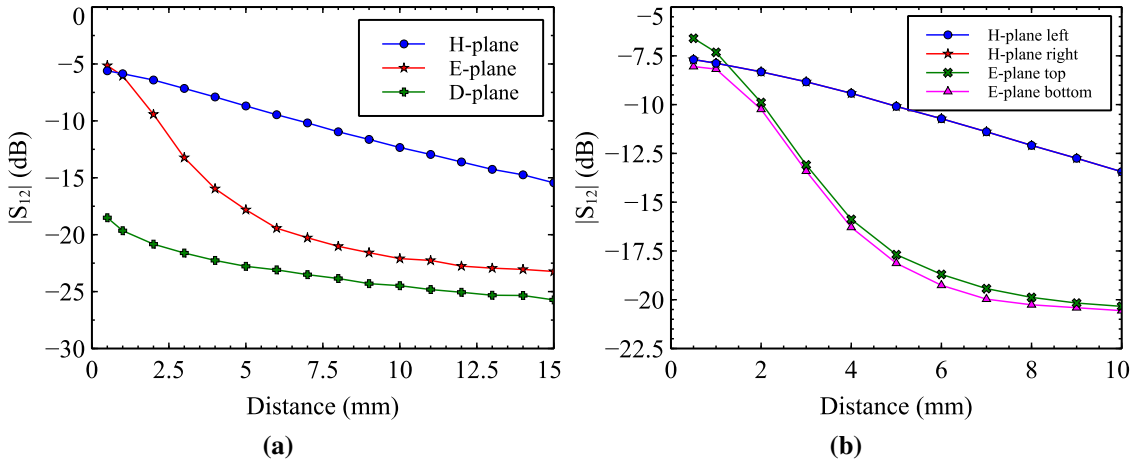

Figure 4.2. (a) Mutual coupling between the driven and one parasitic element in the E-plane and H-plane at 2.45 GHz and (b) Mutual coupling between the driven and two parasitic elements in the E-plane and H-plane at 2.45 GHz.

A square-shaped patch antenna is then simulated with parasitic elements on the right and left side of the driven element for H-plane coupling. For E-plane coupling analysis, the parasitic elements are placed collinearly along the E-plane. Distance between the driven and parasitic elements is varied from 1 mm to 7 mm. For H-plane, it is found that equal coupling is induced between driven and both the parasitic elements. For E-plane, the coupling level is different for top and bottom parasitic elements. From Figure 4.2(b), it can be observed that the coupling strength is different in E-plane and H-plane. The mutual coupling has also been analyzed by keeping the parasitic element in the diagonal plane. However, it is found that the coupling strength in the diagonal plane is minimal as compared to the coupling in E-plane and H-plane for square-shaped elements.

The effect of capacitance values on the mutual coupling and radiation characteristics is analyzed by keeping one tunable parasitic element in the E-plane and H-plane of the square-shaped driven element. For H-plane coupling analysis, the parasitic element is placed on the right-hand side of the driven element. For E-plane coupling analysis, the parasitic element is placed collinearly along the E-plane. The tunable parasitic element is placed at a distance of 3 mm from the driven element, and the capacitance of the varactor diode is varied from 0.84 to 5.08 pF. Minimum mutual coupling between the antenna elements is obtained at 1.82 pF since both the resonant frequencies f_1 and f_2 are not closer to driven element center frequency f. Figure 4.3 and Figure 4.4 depicts the surface current distribution in the E-plane and H-plane for 1.82 and 5.08 pF capacitance, respectively. From the surface current distribution, it can be observed that the minimum current is induced on the tunable parasitic element for 1.82 pF capacitance. Figure 4.5 shows $|S_{12}|$ in the E-plane and H-plane for the capacitance range from 0.84 to 5.08 pF.

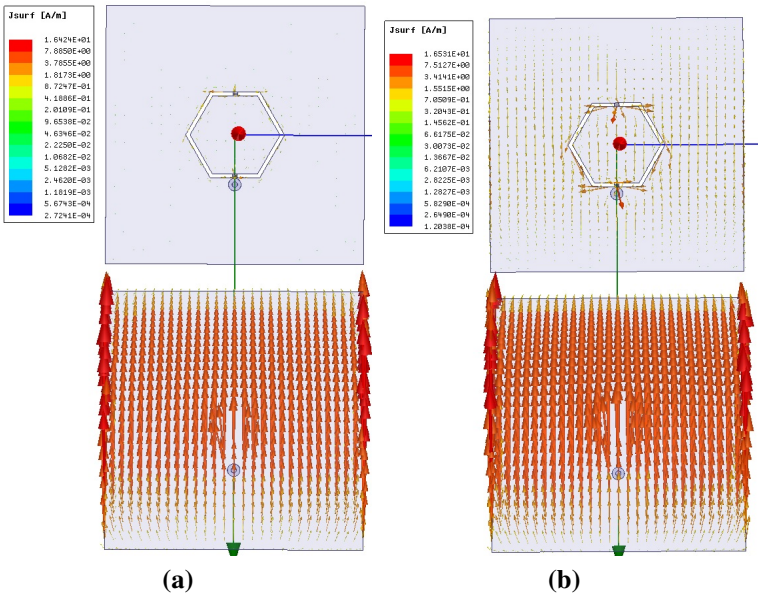

Figure 4.3. Surface current distribution on the driven and tunable parasitic element in the E-plane at 2.45 GHz for capacitance (a) 1.82 pF and (b) 5.08 pF.

For 0.84 pF capacitance, the tunable parasitic element shows strong reflector behavior since $f_1 < f$. The mutual coupling $|S_{12}|$ for 0.84 pF capacitance in the E-plane and H-plane is -16.48 and -12.88 dB respectively. The higher resonating frequency does not cause any effect on the radiation characteristics since $f_2 >> f$. As the capacitance increases from 2.09 to 5.08 pF, the higher resonating frequency f_2 starts approaching f, and as an effect, the coupling between the antenna elements increases. The surface current distribution also shows that strong currents are induced on the tunable parasitic element for 5.08 pF capacitance. The maximum mutual coupling is obtained at 5.08 pF with $|S_{12}|$ as -13.3 dB and -8.67 dB in the E-plane and H-plane respectively. From Figure 4.5, it can be seen that the strength of the mutually coupled field is

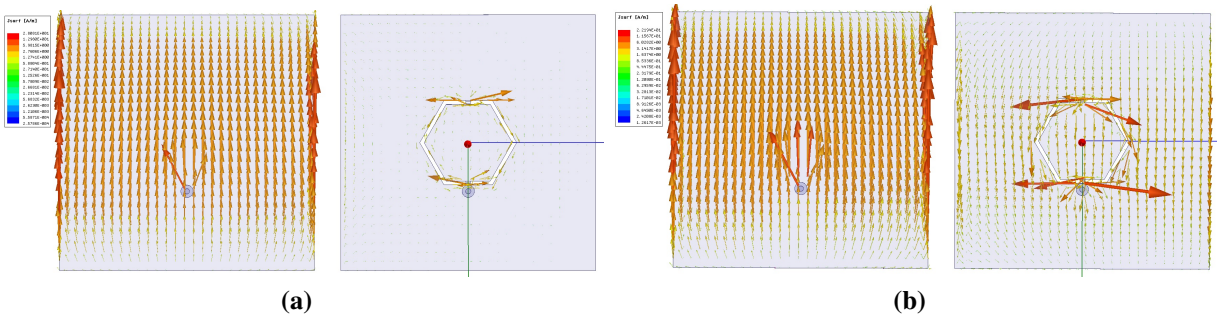

Figure 4.4. Surface current distribution on the driven and tunable parasitic element in the H-plane at 2.45 GHz for capacitance (a) 1.82 pF and (b) 5.08 pF.

different in the E-plane and H-plane. From this analysis on mutual coupling, it is concluded that for 0.84 pF capacitance the tunable parasitic element shows strong reflector characteristics. The director behavior is obtained by using the capacitance from 2.09 to 5.08 pF. The minimum mutual coupling between the antenna elements is obtained at 1.82 pF. These characteristics of tunable parasitic elements are effectively used in the proposed reconfigurable cross parasitic antenna to realize continuous beam scanning in the elevation plane for each azimuthal direction and tunable beamwidth in the E-plane and H-plane.

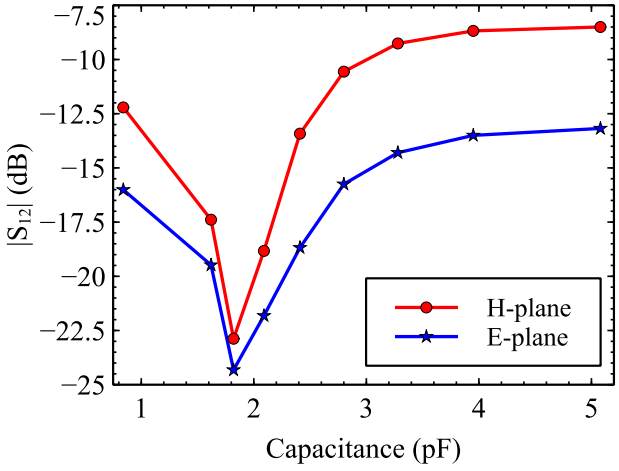

Figure 4.5. Mutual coupling between the driven and tunable parasitic element in E-plane and H-plane at 2.45 GHz for capacitance range from 0.84 to 5.08 pF.

4.2.3 Beamwidth Reconfiguration

In this section, the effect of size of the parasitic element on 3-dB beamwidth is analyzed in both the principal planes by using a three-element parasitic patch antenna configuration. Initially, the two parasitic elements are placed in the E-plane at a distance of 3 mm. The size of the parasitic elements is varied from 21 mm to 41 mm. Figure 4.6 presents beamwidth in the E-plane for

different sizes of the parasitic element. The 3-dB beamwidth of the antenna changes from 44° to 166°, as the size of the parasitic element, is gradually increased from 21 mm to 41 mm. For the physical size from 21 mm to 25 mm, the beamwidth of the antenna is nearly the same as that of an isolated driven element due to weak mutual coupling between the antenna elements. It is observed that highly directional beams are produced when the size of the parasitic element changes from 26 mm to 28.5 mm, and the beamwidth of the antenna starts decreasing from 84° to 44°. The simulation result in HFSS shows that for the physical size of 28.9 mm, 29 mm, and 29.5 mm, a difference beam is obtained since strong currents are induced on the parasitic elements. The 3-dB beamwidth obtained at the physical size of 28.9 mm is 166°. Further increase in the size of the parasitic element shows reflector behavior with a maximum beamwidth of 120°. The simulation result indicated that the overall 3-dB beamwidth of the antenna changes from 44° to 166° for the physical size variation from 21 mm to 41 mm. Lower beamwidth is obtained when the parasitic element shows director behavior. A difference beam with broad beamwidth is observed for nearly equal size of the driven and parasitic element. For this antenna configuration, good impedance matching is achieved at 2.45 GHz with overall bandwidth from 2.43 to 2.47 GHz.

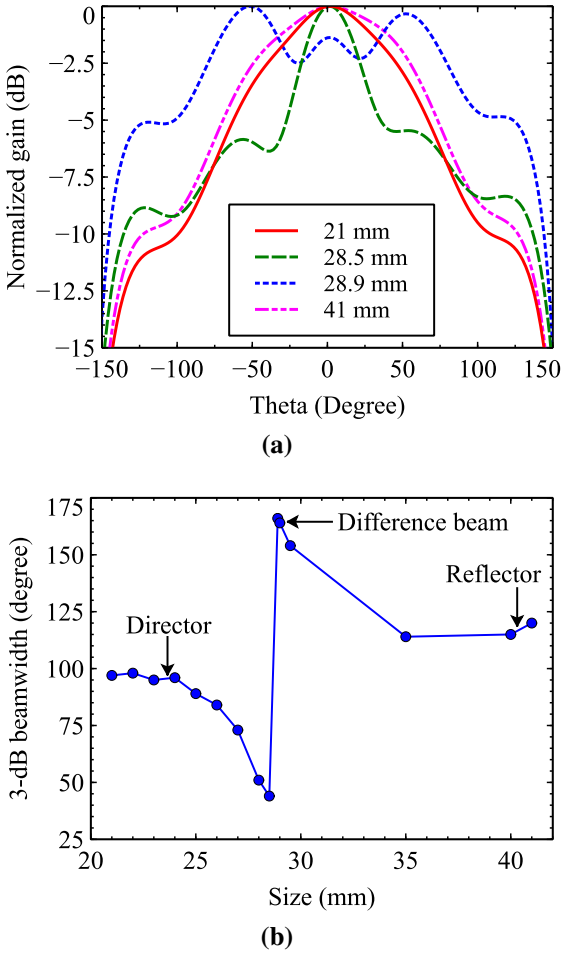

Figure 4.6. Effect of size of the parasitic element placed in the E-plane on 3-dB beamwidth.

The effect of size of the parasitic element on 3-dB beamwidth is also analyzed in the H-plane by using two parasitic elements placed at a distance of 3 mm from the driven element. Size of the parasitic element is varied from 21 mm to 41 mm. As size of the parasitic element increases from 21 mm to 28 mm beamwidth of the antenna decreases from 84° to 58°. Figure 4.7 shows the beamwidth characteristics in the H-plane for different sizes of the parasitic element. For the physical size variation from 35 mm to 41 mm, the antenna shows reflector behavior with maximum beamwidth of 140°. It is observed that the antenna resonates at frequencies higher than 2.45 GHz when size of the parasitic element is very close to the driven element size. Figure 4.8 presents reflection characteristics for the physical size of 28.5 mm, 28.9 mm, and 29 mm. It is difficult to maintain the resonance at 2.45 GHz, due to the strong mutual coupling between the antenna elements. In conclusion, by physically changing the size of the parasitic element from 21 mm to 41 mm, 3-dB beamwidth of the antenna can be varied from 58° to 140°. In the proposed cross parasitic antenna design, tunable parasitic elements are used, which shows dual-band characteristics, and hence size of the parasitic elements can be continuously changed to obtain beamwidth reconfiguration in the E-plane and H-plane.

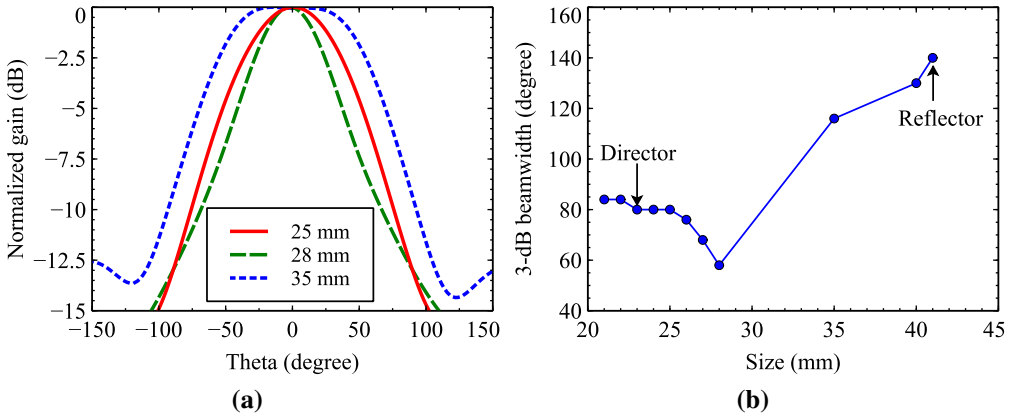

Figure 4.7. Effect of size of the parasitic element placed in the H-plane on 3-dB beamwidth.

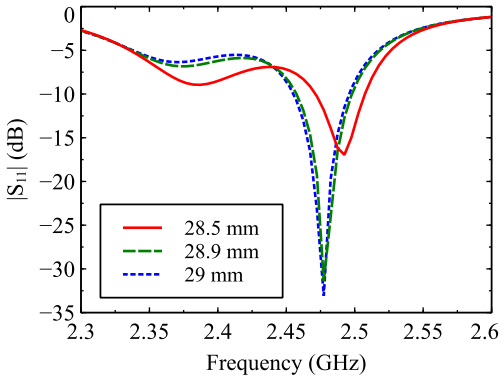

Figure 4.8. Effect of size of the parasitic element placed in the H-plane on reflection characteristics.

4.3 Results and Discussion

The proposed reconfigurable cross parasitic antenna is printed on FR4 substrate of $\epsilon_r = 4.3$, $h = 1.6$ mm and $\tan\delta = 0.02$. Figure 4.9(a) shows a front view of the fabricated antenna. DC voltage to varactor diodes is applied using Keithleys programmable DC power supply and through Coilcraft RF choke coil. RF choke coils are placed on the bottom side of the substrate, as depicted in Figure 4.9(b). The positive terminal of the DC power supply is connected to the cathode of varactor diodes using metallic vias V1, V2, V3, and V4 which are placed at the center of each hexagonal slot. The anode terminal of each varactor diode is grounded through a high impedance transmission line and metallic vias V5, V6, V7, and V8. Reflection and radiation performance of the antenna is measured using Keysight E5063A VNA, as shown in Figure 4.9(c). Figure 4.9(d) shows testing set up used in the anechoic chamber to measure far-field radiation pattern, gain, 3-dB beamwidth, SLL, and cross-polarization.

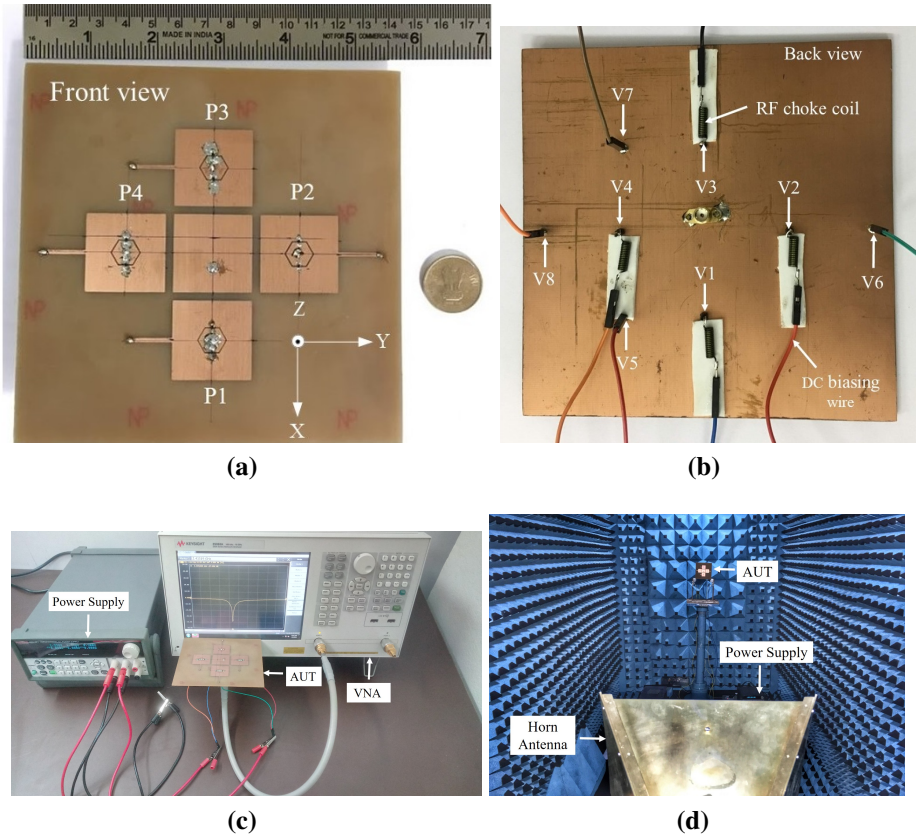

Figure 4.9. Photographs of the fabricated reconfigurable cross parasitic antenna (a) Front view, (b) Back view, (c) Testing of the antenna on VNA and (d) Radiation pattern measurement setup used in the anechoic chamber.

Performance of the proposed reconfigurable cross parasitic antenna is analyzed in five operating modes as follows: a) Broadside mode, b) Minimum coupling ($\phi = 90°$), c) Reflector property ($\phi =$

90°), d) Diagonal plane (ϕ = 45°) and e) E-plane (ϕ = 0°). Table 4.1 shows the capacitance values of the tunable parasitic elements P1, P2, P3, and P4 used in the five operating modes. Effect of different capacitance values on the maximum scanned angle and SLL is analyzed in ϕ = 90° plane by two approaches, minimum mutual coupling, and reflector property. Reflection coefficients are measured in all the operating modes and for all the capacitance values. Overall measured bandwidth of the antenna is found to be from 2.43 to 2.47 GHz. For simplicity, simulated and measured reflection coefficients are shown only for the broadside and minimum coupling operating mode (ϕ = 90°).

Table 4.1. Tunable Parasitic element P1, P2, P3 and P4 capacitance values used in the different operating modes.

Operating mode	P1 (pF)	P2 (pF)	P3 (pF)	P4 (pF)
Broadside	1.82	1.82	1.82	1.82
Minimum coupling ϕ = 90° (H-plane)	1.82	1.82 - 5.08	1.82	1.82
Reflector property ϕ = 90° (H-plane)	1.82	1.62 - 5.08	1.82	0.84
Diagonal plane (ϕ = 45°)	1.82 - 5.08	1.82 - 5.08	1.82	1.82
E-plane (ϕ = 0°)	1.82 - 2.8	1.82	1.82	1.82

4.3.1 Broadside Mode

To obtain broadside radiation, P1, P2, P3, and P4 capacitances are fixed at 1.82 pF by applying a reverse voltage of 3 V. Simulated and measured reflection coefficient displayed in Figure 4.10 shows that the antenna maintains -10 dB impedance bandwidth from 2.43 to 2.47 GHz. The driven element dominates the radiation since mutual coupling between the antenna elements is minimum. Figure 4.11 shows that the main beam of the antenna is steered in the broadside direction. The simulated and measured gain in the broadside mode is 3.18 and 2.65 dBi, respectively. Simulated and measured 3-dB beamwidth is from $-43.2°$ to 43.2° and $-46.8°$ to 50.4°, respectively. Differences in simulation and measured results can be attributed to fabrication tolerance, the insertion loss of SMA connector and the influence of the DC bias lines. Radiation efficiency of the cross antenna is found to be 40%, which is calculated using measured gain and simulated directivity [34]. The lower radiation efficiency of the antenna is significantly caused by the lossy nature of FR4 substrate, mutual coupling, and losses associated with the varactor diode. The radiation efficiency of the antenna can be improved by using low loss microwave substrate and high-quality varactor diodes. Measured cross-polarization level within the 3-dB beamwidth is less than -18.20 dB.

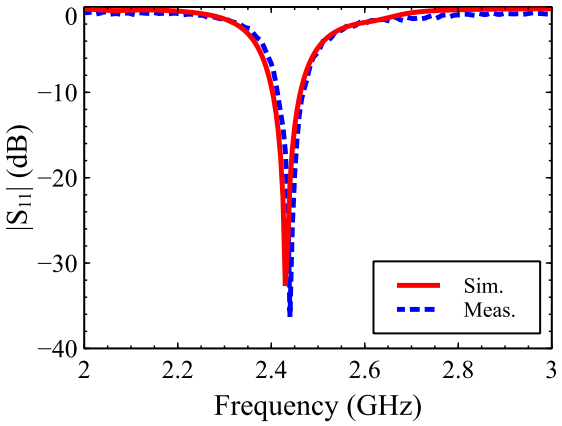

Figure 4.10. Simulated and measured reflection characteristics in the broadside mode.

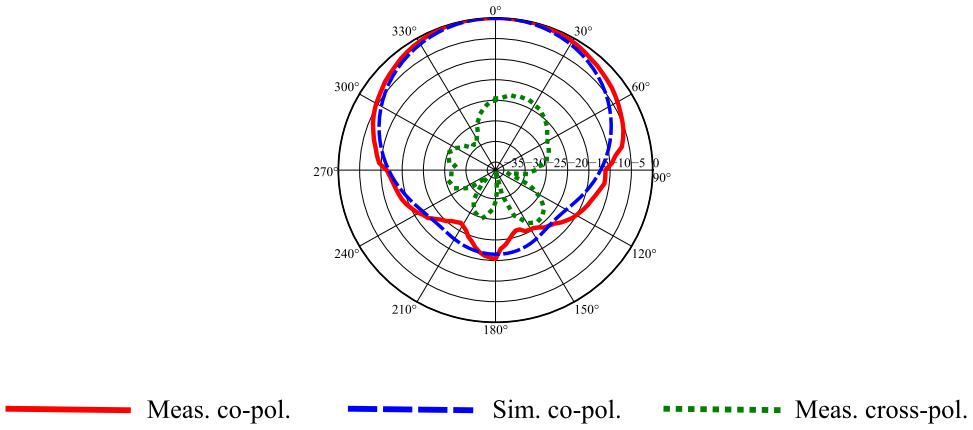

Figure 4.11. Normalized simulated and measured far-field radiation pattern in the broadside mode at 2.45 GHz.

4.3.2 Beam Scanning

This section presents detailed simulation and measured results in the following operating modes: a) Minimum coupling ($\phi = 90°$), b) Reflector property ($\phi = 90°$), c) Diagonal plane ($\phi = 45°$) and d) E-plane ($\phi = 0°$).

4.3.2.1 Minimum Coupling ($\phi = 90°$)

To achieve beam scanning in 90° plane, the capacitance of the parasitic element P2 placed in the H-plane is varied from 1.82 to 5.08 pF. The capacitance of P1, P3, and P4 elements is fixed at 1.82 pF to have minimum mutual coupling. Simulated and measured reflection coefficients presented in Figure 4.12 shows that the antenna maintains impedance matching for all the capacitance values. Simulated and measured far-field radiation patterns for the capacitance range of 1.82 to 5.08 pF

are shown in Figure 4.13. The radiated beam is continuously scanned from 0° to 18°, as the capacitance is varied from 1.82 to 2.8 pF. For the capacitance range of 3.28 to 5.08 pF, the beam is scanned from 25.2° to 32.4° with a maximum measured SLL of −7.3 dB. Measured gain of the antenna varies from 0.17 to 3.02 dBi over the beam scanning range. Variation in gain occurs since the effective electrical size of the antenna is changing with respect to the varactor diode capacitance. The measured 3-dB coverage of the antenna is from −46.8° to 68.4°. Table 4.2 summarizes the detailed simulated and measured results in terms of scanned angle, 3-dB beamwidth, gain, and cross-polarization.

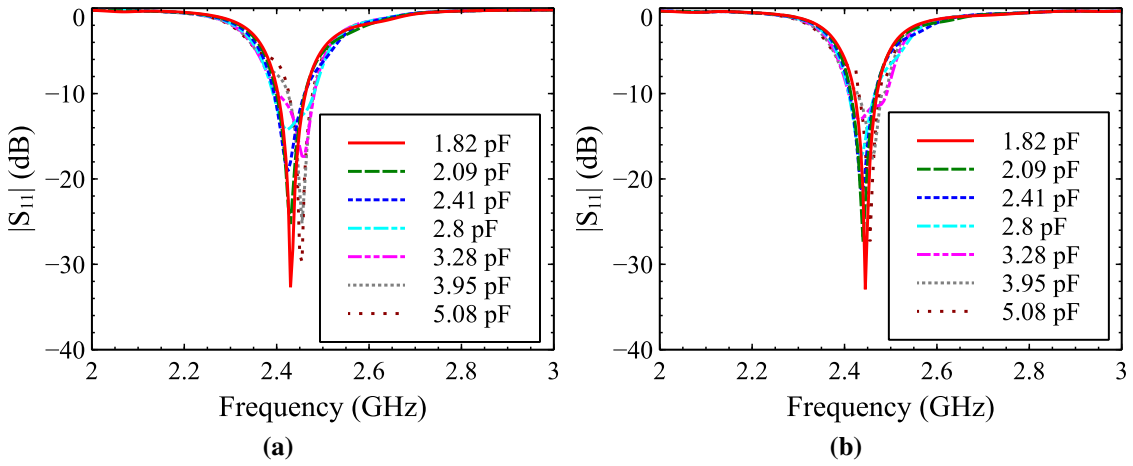

Figure 4.12. Reflection characteristics in minimum coupling (ϕ = 90°) operating mode for capacitance range from 1.82 to 5.08 pF (a) Simulated and (b) Measured.

Table 4.2. Simulated and measured radiation characteristics in minimum coupling (ϕ = 90°) operating mode.

Capacitance (pF)	θ (degree)	3-dB beamwidth (degree)		Gain (dBi)		Cross-polar. (< dB)
	Meas.	Sim.	Meas.	Sim.	Meas.	Meas.
1.82	0	−43.2 - 43.2	−46.8 - 50.4	3.18	2.67	−20.14
2.09	3.6	−36.0 - 43.2	−39.6 - 50.4	3.42	2.85	−19.25
2.41	10.8	−25.2 - 46.8	−28.8 - 54.0	3.43	3.02	−19.19
2.8	18.0	−14.4 - 54.0	−25.2 - 57.6	2.98	1.98	−18.97
3.28	25.2	−3.6 - 61.2	−18.0 - 64.8	2.11	1.60	−18.59
3.95	28.8	0 - 64.8	−3.6 - 72.0	1.20	0.67	−18.15
5.08	32.4	−7.2 - 64.8	0 - 68.4	0.57	0.17	−19.18

4.3.2.2 Reflector Property (ϕ = 90°)

In this operating mode, the parasitic elements P2 and P4 placed in the H-plane are used as director and reflector, respectively. The P2 capacitance is varied from 1.62 to 5.08 pF, and P4 capacitance

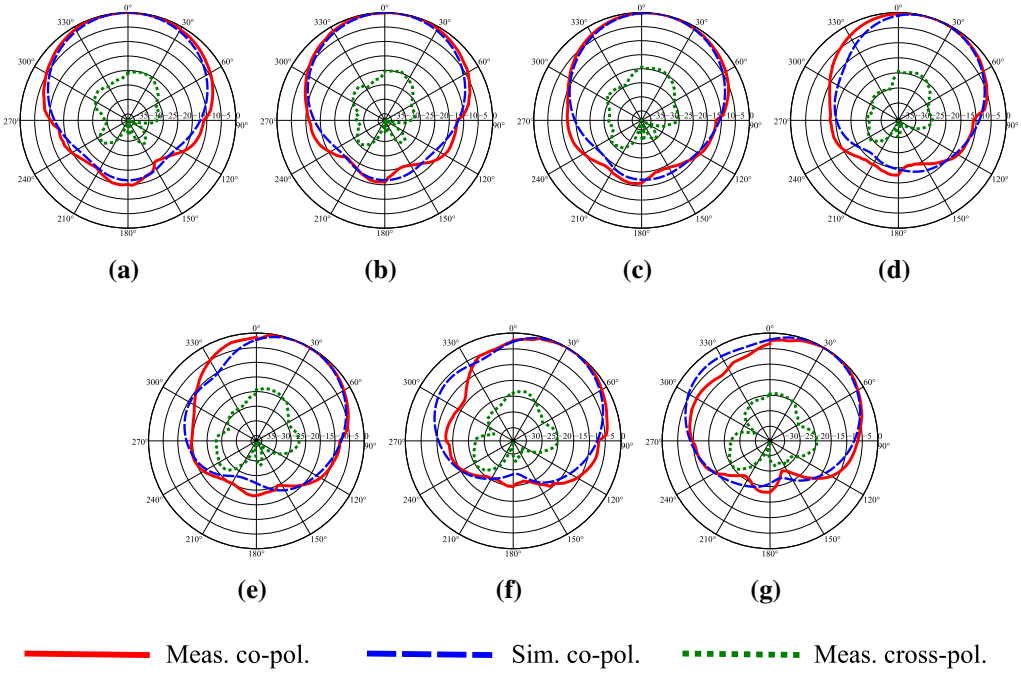

Figure 4.13. Normalized simulated and measured far-field radiation patterns in minimum coupling ($\phi = 90°$) operating mode at 2.45 GHz for capacitance (a) 1.82 pF, (b) 2.09 pF, (c) 2.41 pF, (d) 2.8 pF, (e) 3.28 pF, (f) 3.95 pF and (g) 5.08 pF.

is fixed at 0.84 pF. The capacitance P1 and P3 parasitic elements placed in the E-plane is fixed at 1.82 pF. The simulated and measured reflection characteristics for the capacitance range from 1.62 to 5.08 pF are shown in Figure 4.14. Figure 4.15 shows that the radiated beam is continuously scanned from 3.6° to 40°, as the capacitance is gradually increased from 1.62 to 5.08 pF. Simulated and measured gain of the antenna is in the range of 0.34 to 2.83 dBi and 0.12 to 2.45 dBi, respectively. Measured SLL of the antenna is in the range of -14.02 to -9.2 dB for the capacitance range of 3.28 to 5.08 pF. A more detailed comparison between the simulated and measured results is listed in Table 4.3.

From the measured results in $\phi = 90°$ plane with both the methods, it is concluded that the reflector property of tunable parasitic element helps to increase the beam scanning capability and achieve low SLL. The maximum scanned angle obtained with the reflector property increases from 32.4° to 40°. The SLL obtained with minimum mutual coupling and reflector principle is -7.3 and -9.2 dB, respectively. However, gain, and radiation efficiency with the reflector property decreases due to increased induced current on the parasitic element P2.

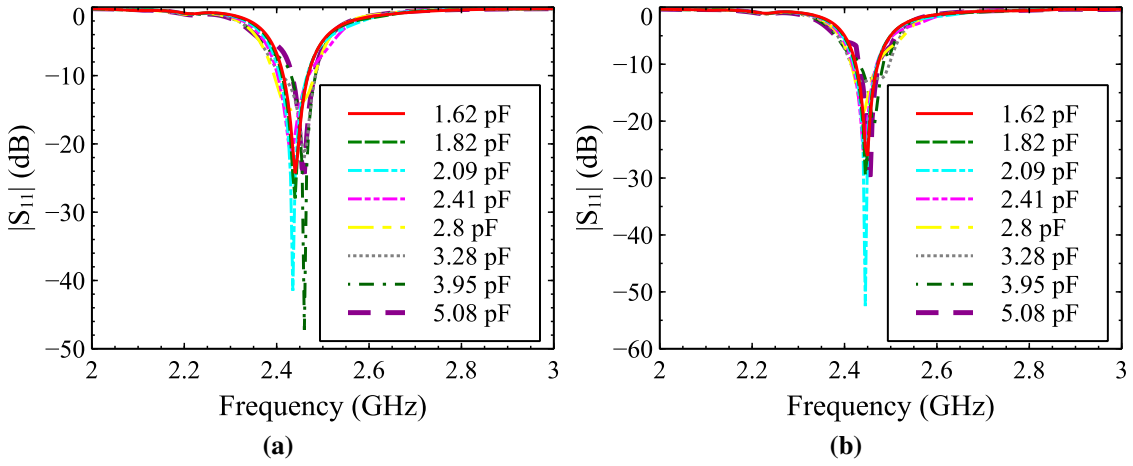

Figure 4.14. Reflection characteristics in reflector property (ϕ = 90°) operating mode for capacitance range from 1.62 to 5.08 pF (a) Simulated and (b) Measured.

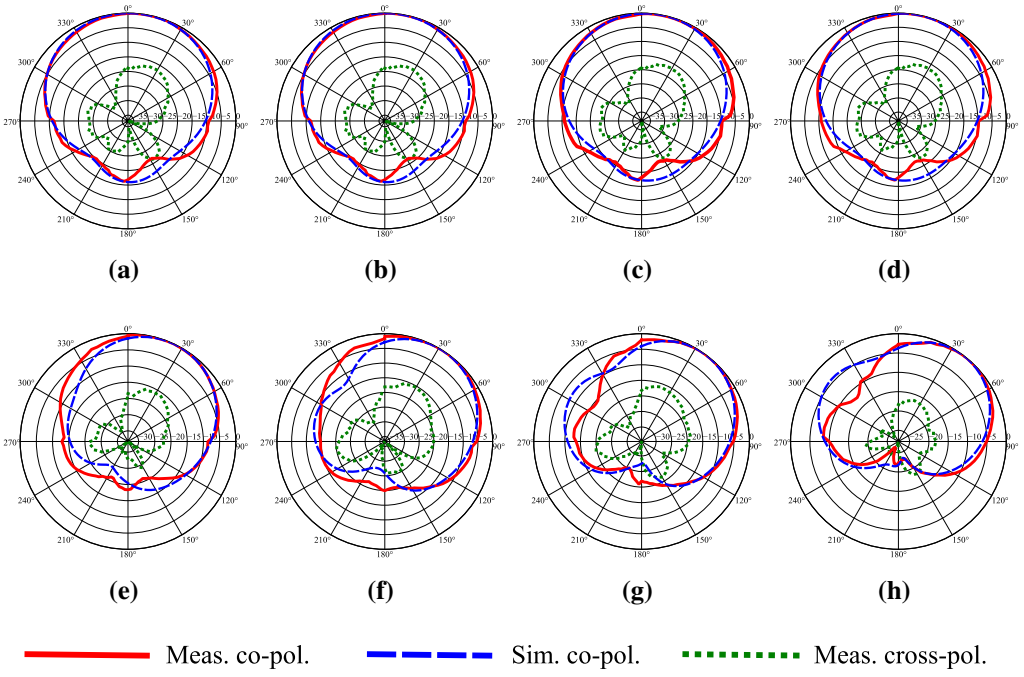

Figure 4.15. Normalized simulated and measured far-field radiation patterns in reflector property (ϕ = 90°) operating mode at 2.45 GHz for capacitance (a) 1.62 pF, (b) 1.82 pF, (c) 2.09 pF, (d) 2.41 pF, (e) 2.8 pF (f) 3.28 pF, (g) 3.95 pF and (h) 5.08 pF.

Table 4.3. Simulated and measured radiation characteristics in reflector property (ϕ = 90°) operating mode.

Capacitance (pF)	θ (degree)	3-dB beamwidth (degree)		Gain (dBi)		Cross-polar. (< dB)
	Meas.	Sim.	Meas.	Sim.	Meas.	Meas.
1.62	3.6	−46.8 - 50.4	−46.8 - 57.6	2.00	1.58	−16.86
1.82	7.2	−43.2 - 50.4	−46.8 - 64.8	2.26	1.80	−17.04
2.09	10.8	−36.0 - 50.4	−36.0 - 64.8	2.66	2.29	−16.72
2.41	14.4	−25.2 - 54.0	−36.0 - 61.2	2.83	2.45	−16.13
2.8	25.2	−10.8 - 61.2	−21.6 - 64.8	2.28	1.25	−16.01
3.28	32.4	0 - 68.4	−7.2 - 75.6	1.72	1.12	−15.48
3.95	36.0	3.6 - 72.0	0 - 75.6	1.02	0.54	−16.17
5.08	40.0	3.6 - 72.0	0 - 75.6	0.34	0.12	−16.51

4.3.2.3 Diagonal Plane (ϕ = 45°)

Continuous beam scanning in the diagonal plane is realized by varying the capacitance of tunable parasitic elements placed in the E-plane and H-plane. To achieve beam scanning in ϕ = 45° plane, P1, and P2 parasitic capacitances are simultaneously varied from 1.82 to 5.08 pF. The P3 and P4 parasitic patch capacitances are fixed at 1.82 pF. Figure 4.16 presents the simulated and measured reflection characteristics. Main beam of the antenna is continuously scanned from 3.6° to 32.4° with 3-dB coverage from −39.6° to 75.6°. Figure 4.17 shows the normalized simulated and measured far-field radiation patterns. Measured gain of the antenna is in the range of 0.43 to 3.27 dBi. Measured SLL obtained at 5.08 pF is −9.6 dB. Table 4.4 summarizes detailed simulation and measured results.

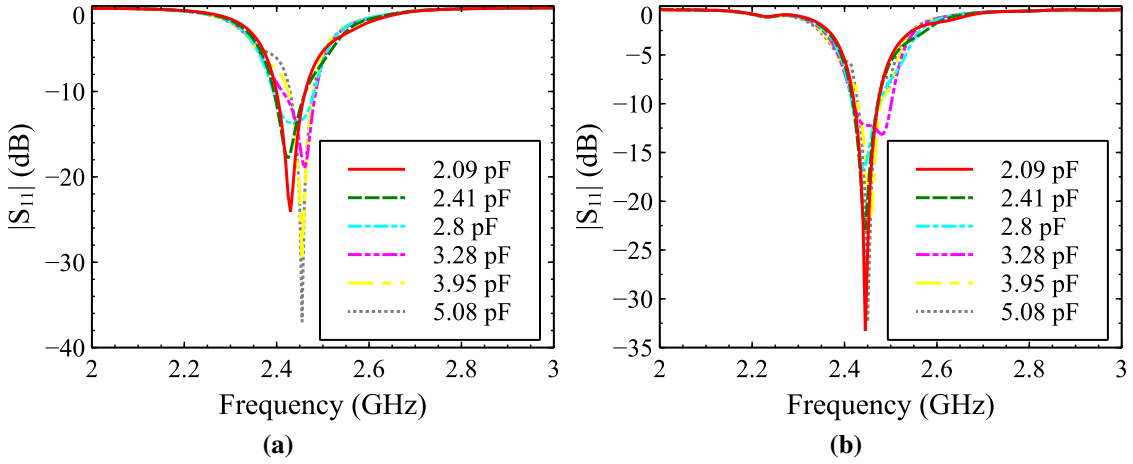

Figure 4.16. Reflection characteristics in ϕ = 45° operating mode for capacitance range from 2.09 to 5.08 pF (a) Simulated and (b) Measured.

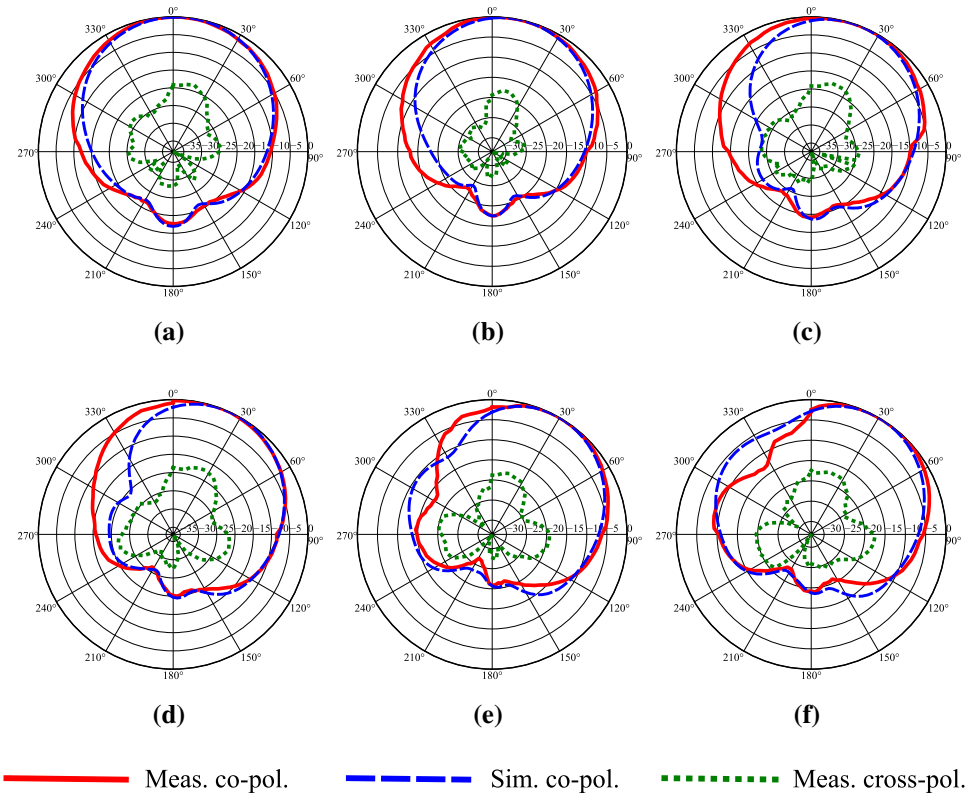

Figure 4.17. Normalized simulated and measured far-field radiation patterns in $\phi = 45°$ plane at 2.45 GHz for capacitance (a) 2.09 pF, (b) 2.41 pF, (c) 2.8 pF, (d) 3.28 pF, (e) 3.95 pF and (f) 5.08 pF.

Table 4.4. Simulated and measured radiation characteristics in $\phi = 45°$ plane.

Capacitance (pF)	θ (degree)	3-dB beamwidth (degree)		Gain (dBi)		Cross-polar. ($<$ dB)
	Meas.	Sim.	Meas.	Sim.	Meas.	Meas.
2.09	3.6	−32.4 - 43.2	−39.6 - 46.8	3.62	2.98	−18.37
2.41	10.8	−25.2 - 46.8	−32.4 - 54.0	3.78	3.27	−18.02
2.8	18.0	−10.8 - 54.0	−28.8 - 61.2	2.89	2.11	−17.63
3.28	25.2	−3.6 - 61.2	−21.6 - 61.2	1.81	1.58	−17.35
3.95	28.8	0 - 64.8	−7.2 - 68.4	1.12	0.92	−17.88
5.08	32.4	0 - 64.8	0 - 75.6	0.84	0.43	−17.25

4.3.2.4 E-plane (ϕ = 0°)

In ϕ = 0° plane, P1 parasitic patch capacitance is varied from 1.82 to 2.8 pF. The capacitance of tunable parasitic elements P2 and P4 is fixed at 1.82 pF. From Figure 4.18 it can be seen that the antenna shows good impedance matching for the capacitance range from 2.09 to 2.8 pF. The radiated beam is continuously scanned from 3.6° to 10.8°, as shown in Figure 4.19. Detailed simulation and measured results are presented in Table 4.5. It is observed that for higher capacitance values, the proposed cross parasitic antenna does not show any improvement in beam scanning. It is very difficult to scan the radiated beam above 10.8° in the E-plane due to reasons such as a) Difference in coupling levels of E-plane and H-plane [72] b) Amplitude of the coupled field is different for top and bottom parasitic element in the E-plane [159] and c) Induced currents on the driven and parasitic elements are out of phase in the E-plane [160].

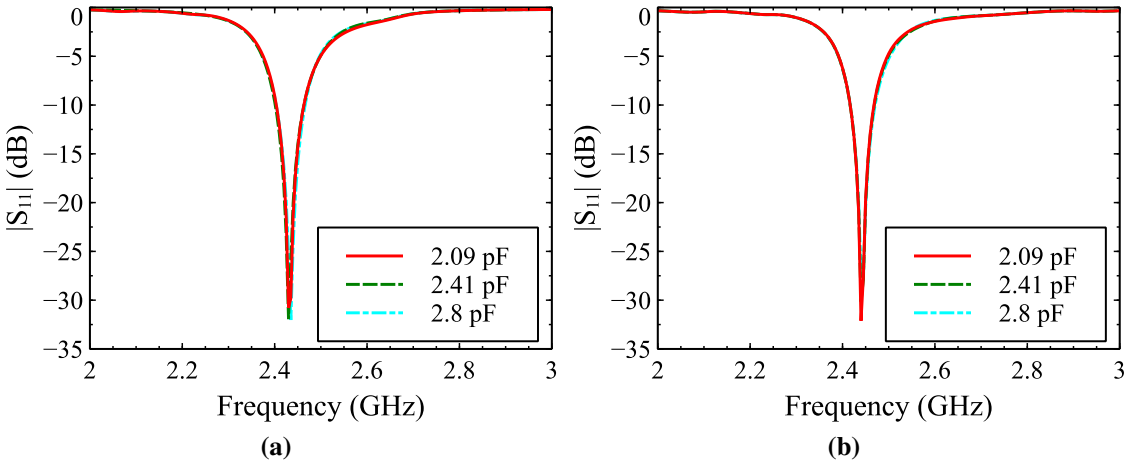

Figure 4.18. Reflection characteristics in ϕ = 0° operating mode for capacitance range from 2.09 to 2.8 pF (a) Simulated and (b) Measured.

Table 4.5. Simulated and measured radiation characteristics in ϕ = 0° plane.

Capacitance (pF)	θ (degree)	3-dB beamwidth (degree)		Gain (dBi)		Cross-polar. (< dB)
	Meas.	Sim.	Meas.	Sim.	Meas.	Meas.
2.09	3.6	−36.0 - 54.0	−39.6 - 50.4	3.38	2.97	−18.25
2.41	7.2	−32.4 - 54.0	−36.0 - 57.6	3.52	3.18	−18.46
2.8	10.8	−28.8 - 57.6	−32.4 - 57.6	2.99	2.32	−18.98

Simulated and measured results of the proposed reconfigurable cross parasitic antenna are presented in three azimuth planes ϕ = 0°, 45° and 90°. Similar radiation characteristics can be obtained in the remaining planes by properly selecting capacitances of tunable parasitic elements, as presented in Table 4.6.

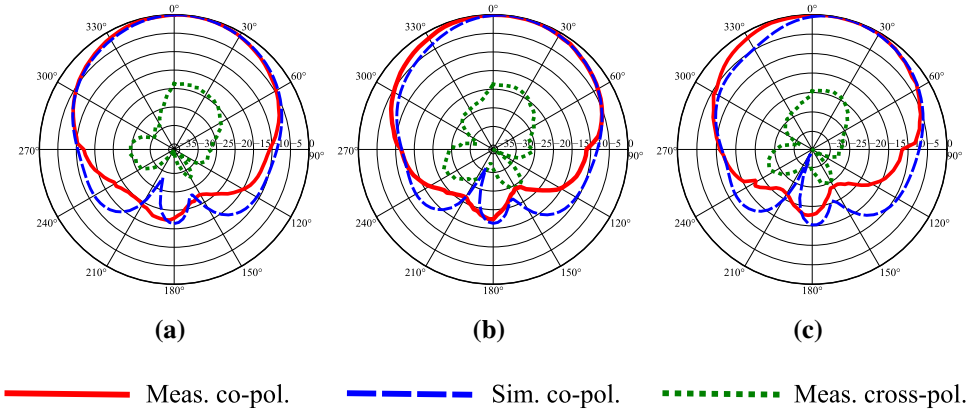

Figure 4.19. Normalized simulated and measured far-field radiation patterns in $\phi = 0°$ plane at 2.45 GHz for capacitance (a) 2.09 pF, (b) 2.41 pF and (c) 2.8 pF.

Table 4.6. Tunable parasitic element P1, P2, P3 and P4 capacitance values used to realize continuous beam scanning in $\phi = 135°$, 180°, 225°, 270° and 315° planes.

ϕ (degree)	P1 (pF)	P2 (pF)	P3 (pF)	P4 (pF)
135	1.82	1.82 - 5.08	1.82 - 5.08	1.82
180	1.82	1.82	1.82 - 2.8	1.82
225	1.82	1.82	1.82 - 5.08	1.82 - 5.08
270	1.82	0.84	1.82	1.62 - 5.08
315	1.82 - 5.08	1.82	1.82	1.82 - 5.08

Figure 4.20 shows the Three-Dimensional (3-D) polar patterns in eight azimuthal directions, ϕ = 0° (θ = 10.8°), 45° (θ = 32.4°), 90° (θ = 40°), 135° (θ = 32.4°), 180° (θ = 10.8°), 225° (θ = 32.4°), 270° (θ = 40°) and 315° (θ = 32.4°) planes. The 3-D radiation pattern is plotted by selecting the maximum value of θ in the corresponding azimuth plane. The 3-D radiation pattern is also plotted in the reflector property (ϕ = 90°) operating mode, as shown in Figure 4.21. In this operating mode, the main beam of the antenna is continuously scanned from 3.6° to 40°, as the capacitance is varied from 1.62 to 5.08 pF.

4.3.3 Tunable Beamwidth

For tunable beamwidth in the E-plane (ϕ = 0°) and H-plane (ϕ = 90°), reflector, director and neutral behavior of the parasitic element is used. The antenna shows unidirectional radiation characteristics in both the planes with the main beam is always directed to 0° for all the capacitance values.

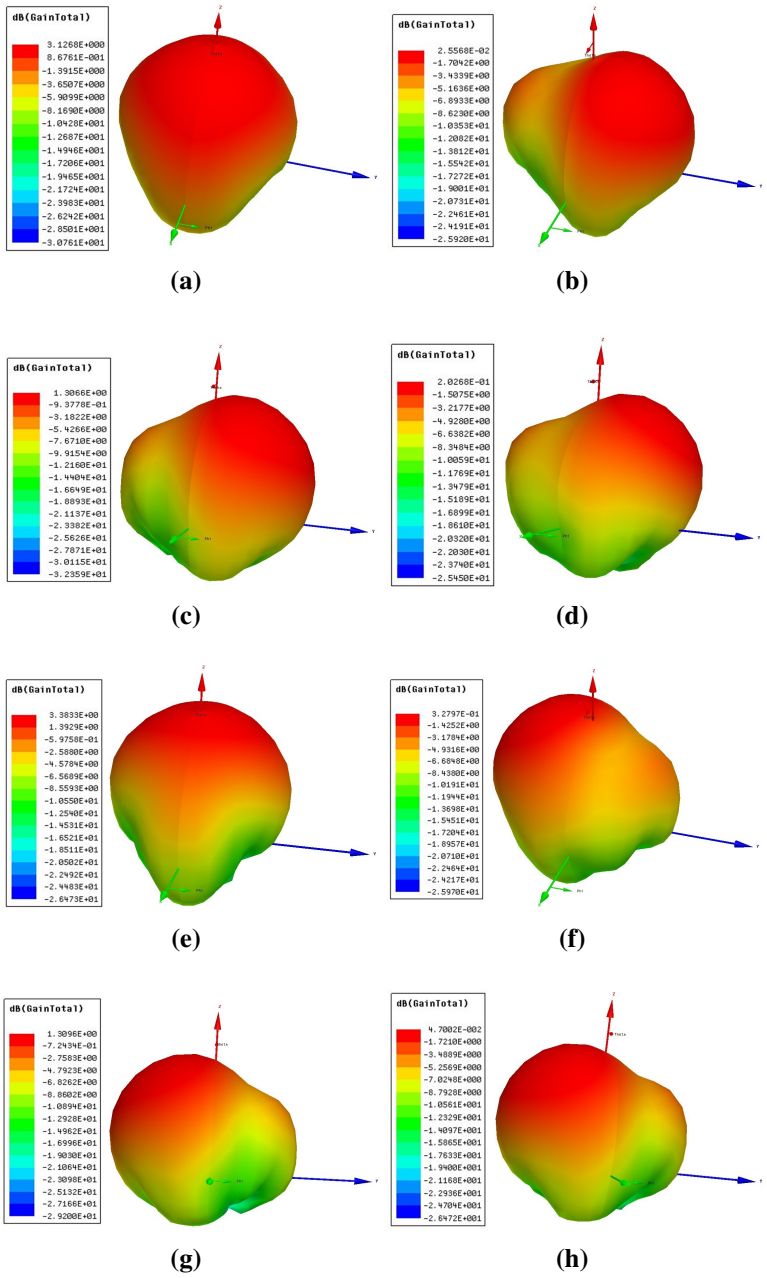

Figure 4.20. 3-D polar patterns for (a) $\phi = 0°$ ($\theta = 10.8°$), (b) $\phi = 45°$ ($\theta = 32.4°$), (c) $\phi = 90°$ ($\theta = 40°$), (d) $\phi = 135°$ ($\theta = 32.4°$), (e) ϕ =180° ($\theta = 10.8°$), (f) $\phi = 225°$ ($\theta = 32.4°$), (g) $\phi = 270°$ ($\theta = 40°$) and (h) $\phi = 315°$ ($\theta = 32.4°$).

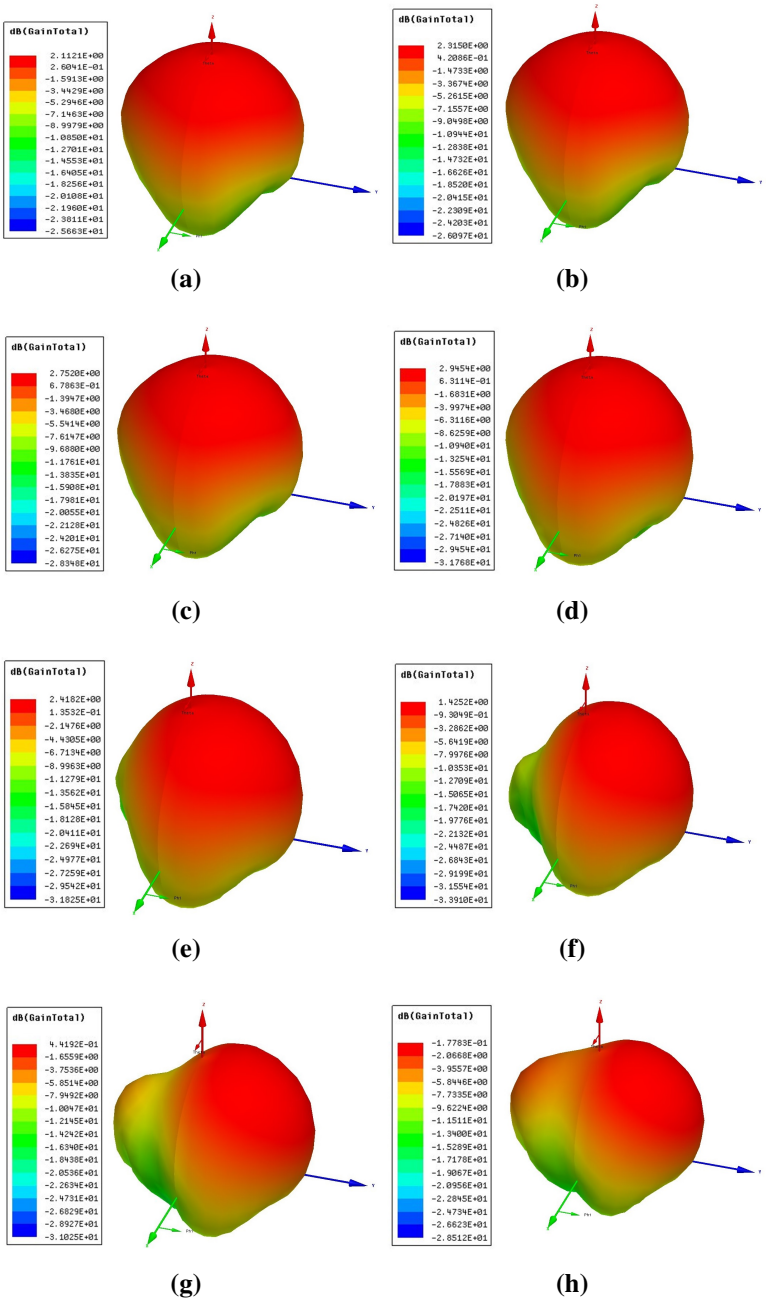

Figure 4.21. 3-D polar patterns for reflector property ($\phi = 90°$) operating mode for the capacitance (a) 1.62 pF, (b) 1.82 pF, (c) 2.09 pF, (d) 2.41 pF, (e) 2.8 pF, (f) 3.28 pF, (g) 3.95 pF and (h) 5.08 pF.

4.3.3.1 E-plane (ϕ = 0°)

To realize continuous beamwidth tuning in E-plane, P1 and P3 parasitic element is simultaneously used as either reflector or director. The parasitic elements P2 and P4 placed in the H-plane are fixed at 1.82 pF to have minimum mutual coupling. The capacitance on P1 and P3 elements is varied from 0.84 to 3.95 pF. For all capacitance values, the antenna shows excellent impedance matching with $|S_{11}| \leq -21$ dB, as shown in Figure 4.22. For 0.84 pF capacitance, P1 and P3 show strong reflector characteristics, and the antenna achieves a broad beamwidth of 118°. For 1.82 pF capacitance, the beamwidth of the antenna is 101°, which is nearly the same as that of a single square-shaped driven element. For the capacitance range from 2.09 to 2.8 pF, the tunable parasitic element shows director behavior, and the radiated beam becomes more directional. Measured beamwidth of the antenna for this capacitance range decreases from 87° to 65°. Figure 4.23 and Figure 4.24 presents the simulated and measured tunable beamwidth results for the capacitance from 0.84 to 3.95 pF, respectively.

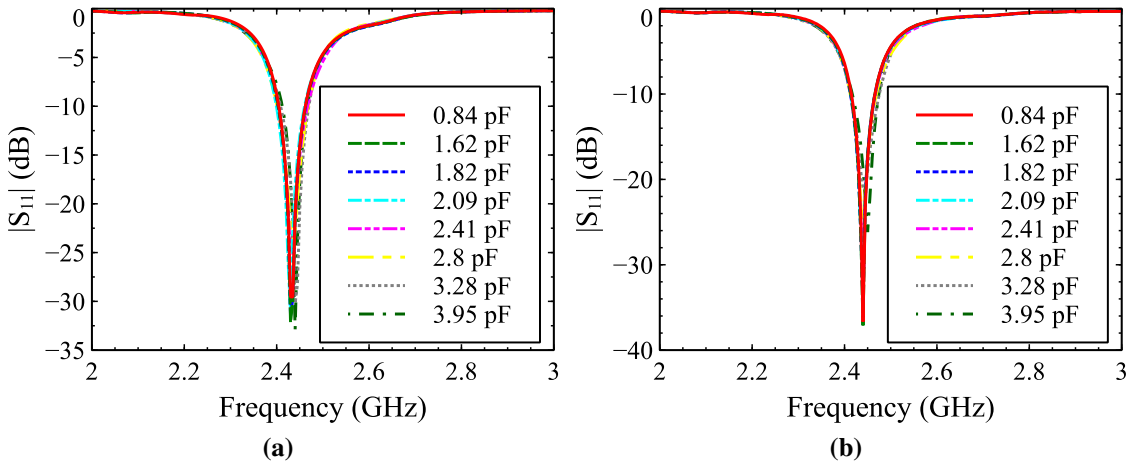

Figure 4.22. Reflection coefficient for tunable beamwidth configuration in the E-plane for capacitance range from 0.84 to 3.95 pF (a) Simulated and (b) Measured.

For 3.95 pF capacitance, the difference beam is obtained with a broad beamwidth of 152°. Surface current distribution for capacitance 3.28 pF and 3.95 pF is shown in Figure 4.25. It is observed that the current induced on the tunable parasitic elements placed in the E-plane increases, as the capacitance is varied from 3.28 to 3.95 pF. Due to symmetry of the proposed cross parasitic antenna, the induced currents on the parasitic elements are equal with each other but different from the driven element. In [92], it has been shown that for such an even distribution of amplitude (α) and phase (β) around the driven element, difference beam exists at some α/β values. The simulated directivity of the antenna in the E-plane is found to be in the range of 5.92 to 7.96 dB. Measured cross-polarization is less than -16.59 dB throughout the beamwidth tuning range. Table

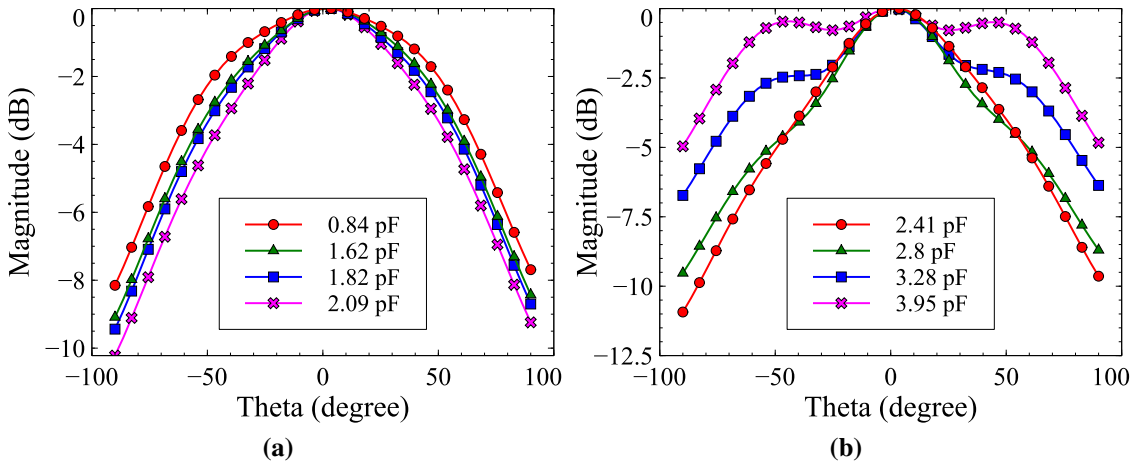

Figure 4.23. Simulated tunable beamwidth in the E-plane at 2.45 GHz for capacitance (a) 0.84 to 2.09 pF and (b) 2.41 to 3.95 pF.

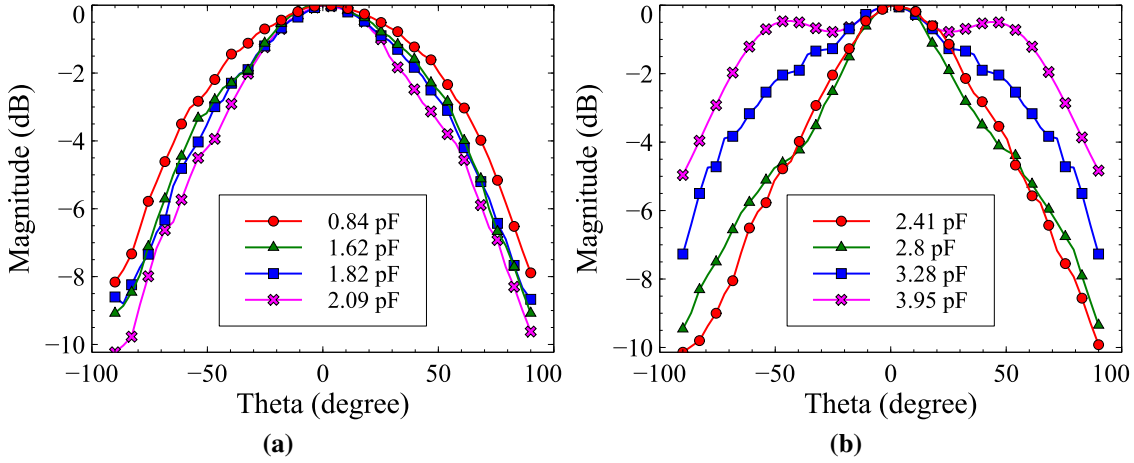

Figure 4.24. Measured tunable beamwidth in the E-plane at 2.45 GHz for capacitance (a) 0.84 to 2.09 pF and (b) 2.41 to 3.95 pF.

4.7 summarizes detailed simulated and measured results in the E-plane. The antenna shows stable radiation characteristics in the H-plane with an average 3-dB beamwidth of 80°. Measured peak gain of 3.22 dBi is observed with a gain variation of 3.01 dB along the entire beamwidth tuning range.

4.3.3.2 H-plane (ϕ = 90°)

Beamwidth reconfiguration characteristics are also verified in H-plane by varying P2 and P4 capacitance from 0.84 to 2.8 pF. The capacitance of parasitic elements placed in the E-plane is fixed at 1.82 pF. Simulated and measured overall impedance bandwidth for the capacitance range of 0.84 to 2.8 pF is from 2.43 to 2.47 GHz, as shown in Figure 4.26. It is observed that the

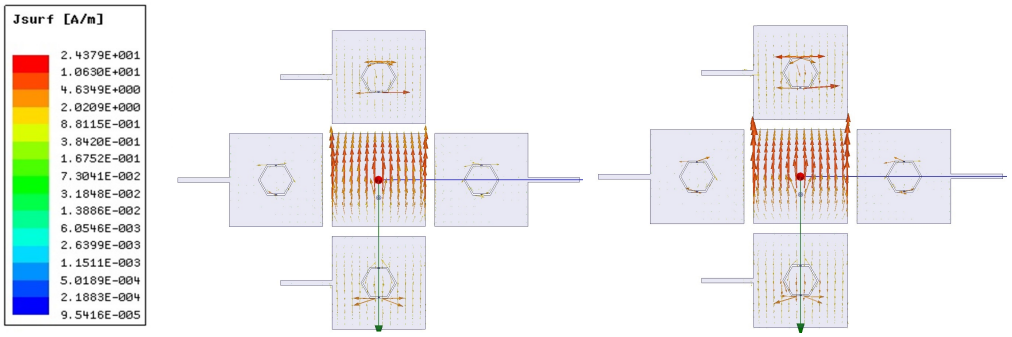

Figure 4.25. Surface current distribution on the driven and tunable parasitic elements for tunable beamwidth configuration in the E-plane at an operating frequency of 2.45 GHz for capacitance (a) 3.28 pF and (b) 3.95 pF.

Table 4.7. Simulated and measured results for tunable beamwidth configuration in the E-plane at 2.45 GHz.

Capacitance (pF)	3-dB beamwidth (degree)		Gain (dBi)		Directivity (dB)	Cross-polar. (< dB)
	Sim.	Meas.	Sim.	Meas.	Sim.	Meas.
0.84	−57 - 59 (116)	−57 - 61 (118)	2.29	1.88	6.68	−16.59
1.62	−50 - 54 (104)	−50 - 54 (104)	2.86	2.14	7.03	−17.35
1.82	−47 - 52 (99)	−47 - 54 (101)	3.08	2.65	7.16	−17.15
2.09	−40 - 47 (87)	−40 - 47 (87)	3.47	2.88	7.48	−17.26
2.41	−32 - 42 (74)	−32 - 40 (72)	3.73	3.22	7.85	−17.70
2.80	−29 - 35 (64)	−29 - 36 (65)	2.79	2.30	7.96	−17.46
3.28	−59 - 61 (120)	−61 - 61 (122)	0.97	0.50	7.12	−17.99
3.95	−76 - 76 (152)	−76 - 76 (152)	0.53	0.21	5.92	−20.01

resonance is shifted to the higher frequency for the capacitance range of 3.28 to 5.08 pF. Shifting in resonance mainly occurs due to the strong mutual coupling between the antenna elements placed in the H-plane. Deviation in resonance is not observed in the E-plane since coupling in E-plane is smaller as compared to H-plane for the square-shaped microstrip elements. It is observed from Figure 4.27 that the measured beamwidth of the antenna decreases from 116° to 64°, as the capacitance is varied from 0.84 to 2.8 pF. Measured cross-polarization in the H-plane is found to be less than −16.04 dB throughout the beamwidth tuning range. A stable broadside radiation pattern is observed in the E-plane with an average 3-dB beamwidth of 102°. Simulated directivity is in the range of 6.32 to 7.61 dB. Measured gain in the H-plane varies from 0.52 to 3.02 dBi. Detailed simulated and measured results are presented in Table 4.8.

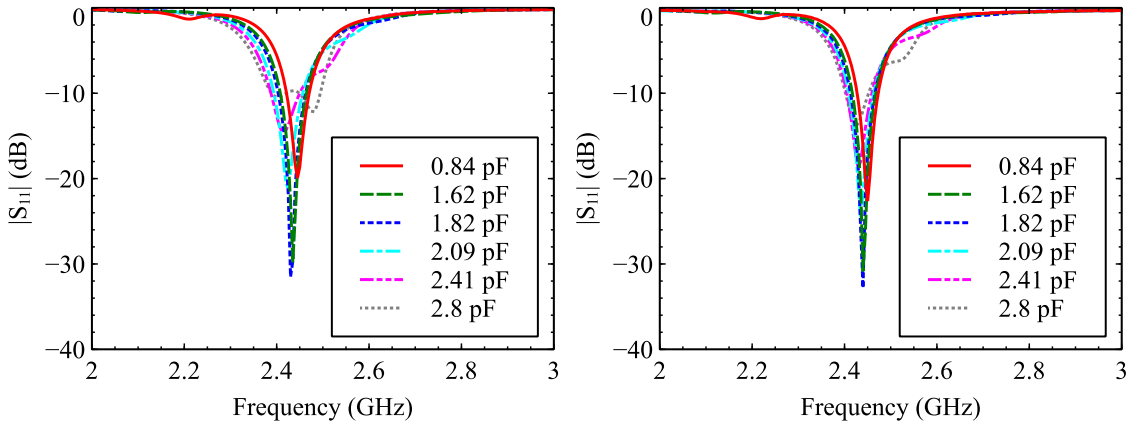

Figure 4.26. Reflection coefficient for tunable beamwidth configuration in the H-plane for capacitance range from 0.84 to 2.8 pF (a) Simulated and (b) Measured.

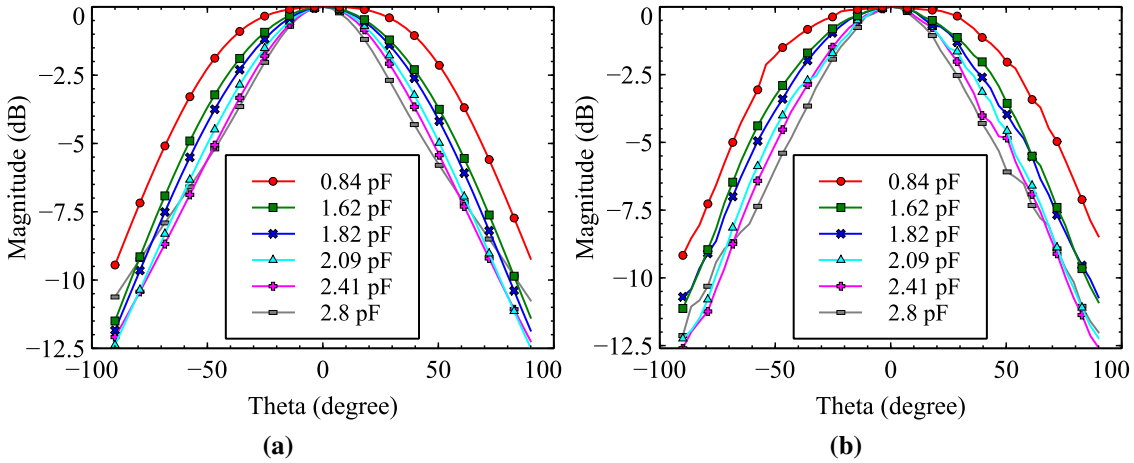

Figure 4.27. Tunable beamwidth in the H-plane at 2.45 GHz for capacitance range from 0.84 to 2.8 pF (a) Simulated and (b) Measured.

Table 4.8. Simulated and measured results for tunable beamwidth configuration in the H-plane at 2.45 GHz.

Capacitance (pF)	3-dB beamwidth (degree)		Gain (dBi)		Directivity (dB)	Cross-polar. (< dB)
	Sim.	Meas.	Sim.	Meas.	Sim.	Meas.
0.84	−56 - 56 (112)	−58 - 58 (116)	0.86	0.52	6.32	−16.04
1.62	−45 - 45 (90)	−47 - 47 (94)	2.62	2.08	6.98	−16.98
1.82	−41 - 41 (82)	−43 - 43 (86)	3.08	2.65	7.15	−17.60
2.09	−37 - 37 (74)	−40 - 40 (80)	3.58	2.79	7.42	−17.74
2.41	−34 - 34 (68)	−36 - 36 (72)	3.55	3.02	7.57	−17.91
2.8	−31 - 31 (62)	−32 - 32 (64)	2.26	2.00	7.61	−18.49

4.3.4 Performance Comparison

The performance of the proposed reconfigurable cross parasitic antenna is compared with the other reported designs [24, 25, 73, 74, 92, 103, 104] in terms of size, a number of parasitic elements, operating bandwidth, beam coverage, peak gain, and 3-dB beamwidth. A detailed performance comparison is presented in Table 4.9. The proposed reconfigurable cross parasitic antenna design overcomes the limitations of existing parasitic antennas in terms of limited coverage in the horizontal plane [73, 92, 103, 104], discrete beam switching in [24, 25, 73, 74, 104], beamwidth tuning in H-plane alone [92] and beamwidth tuning with limited beam scanning in H-plane [103]. From Table 4.9, it can be seen that the proposed antenna is able to achieve continuous variation in the radiated beam and 3-dB beamwidth. All the other reported antenna designs achieve discrete variation in radiation characteristics. The antenna designs presented in [24, 73, 74] attained pattern reconfiguration with fixed beamwidth. In [104], continuous beam scanning, as well as beamwidth tuning in the H-plane is realized with enhanced bandwidth. However, the use of an air gap to enhance bandwidth increases the size and profile of the antenna.

4.4 Summary

A multifunctional reconfigurable cross parasitic antenna is presented to cover the entire azimuth plane and achieve tunable beamwidth in the E-plane and H-plane. The proposed cross parasitic antenna consists of a square-shaped driven element with four tunable parasitic elements placed in the E-plane and H-plane. This antenna has the capability of achieving continuous beam scanning and beamwidth tuning in a single antenna structure. Mutual coupling is analyzed in detail by keeping the parasitic element in the E-plane and H-plane of the driven element. The radiated beam is continuously scanned in the elevation plane from 0° to 10.8°, 0° to 32.4° and 0° to 40° in E-plane, diagonal plane and H-plane respectively. Furthermore, 3-dB beamwidth of the cross antenna is continuously tuned from 65° to 152° and 64° to 116° in the E-plane and H-plane respectively. The antenna has the advantages of simple design, low profile, a planar structure, and maintained impedance characteristics in all the operating modes. In the next chapter, RA design is presented to achieve the independent pattern, beamwidth, and polarization reconfiguration in a single antenna structure.

Table 4.9. Performance comparison of the proposed reconfigurable cross parasitic antenna with other reported designs.

Reference	Size (mm^3) (λ_0^3)	Substrate	Number of parasitic elements	Operating bandwidth (%)	360° azimuth coverage	Main beam elevation plane (degree)	Peak gain (dBi)	3-dB beamwidth (degree)	Switches (number)	Steering type
[73]	1.03×1.03×0.013	Taconic	4	1.68	No	15	8.20	58	PIN (4)	discrete
[74]	0.95×0.95×0.013	Taconic	4	1.26	Yes	25	8.01	55	PIN (4)	discrete
[24]	0.74×0.80×0.1	Rogers	9	4.08	Yes	30	6.50	n/a	PIN (12)	discrete
[92]	1.65×0.82×0.026	Rogers	2	2.00	No	Broadside	8.60	50 to 112 (H-plane)	varactor (2)	continuous
[103]	1.50×1.40×n/a	Rogers	2	6.40	No	20	8.80	60 to 130 (H-plane)	varactor (2)	continuous
[104]	1.17×1.17×0.08	Rogers	2	5.56	No	−17, 14	7	49, 105	PIN (8)	discrete
[25]	1×1×0.18	Rogers	2	4	Yes	±40	8	40 (E-plane) 100 (H-plane) 100 (D-plane)	PIN (6)	discrete
Proposed	1.14×1.14×0.013	FR4	4	1.63	Yes	10.8 (E-plane) 40 (H-plane)	3.78	65 to 152 (E-plane) 64 to 116 (H-plane)	varactor (8)	continuous